OPEN ACCESS
Saudi Journal of Biomedical Research
Abbreviated Key Title: Saudi J Biomed Res
ISSN 2518-3214 (Print) |ISSN 2518-3222 (Online)
Scholars Middle East Publishers, Dubai, United Arab Emirates
Journal homepage: http://scholarsmepub.com/sjbr/

Original Research Article

Experimental Analysis of Deformations in Artificial Jaw Bone by Means of an Interferometry Technique

B. Trentadue*
DMMM, Politecnico di Bari- Viale Japigia 182 - 70126 Bari, Italy

***Corresponding author:** B. Trentadue
| **Received:** 01.02.2019 | **Accepted:** 11.02.2019 | **Published:** 19.02.2019
DOI:10.21276/sjbr.2019.4.2.2

Abstract

The present work studied experimental results obtained on an artificial mandibular bone in according to tests carried out on live animals. In particular, in order to consider the dynamic response of an implant bridge caused by occlusion, the deformation of the bridge and the near mandible subjected to occlusional force was measured by holographic interferometry. An experimental specimen was built for the above purpose and a screw type ceramic implant was placed in the site of the second molar. An implant bridge was then fabricated between the implant and the first and second premolars that were splinted together. Stress concentration was found on the mesial side of the pontic when the vertical load was applied to the second premolar. The results also show that by applying the load to its mesial side, the mandible near the implant receives considerable stress and of course damages such as bone resorption can be expected on the mandible. The principal strains on the surface of the mandibular bone were tensile and compressive strains from anteroinferior to posterosuperior and a compressive strain from anterosuperior to posteroinferior.

Keywords: deformation, mandible, premolar.

INTRODUCTION

As regards the installation of dental prosthesis, fixed ones are certainly more convenient than removable ones in terms of masticatory efficiency, patient relief and reliability.

The research developed in the bio-mechanic field has carried out, in recent years, several new techniques focused on a more acceptable integration of the prosthesis in the patient bone.

While the creation of new bio-materials has truly reached a high level of quality and similarity with bone and tooth materials, there continues to be a gap in the mandible dynamic responses compared to the existent case of natural teeth. This is due to the absence of periodontal fibers that are absolutely necessary to attenuate the strong masticatory forces.

The intention of this research was to mainly test, on human beings, the junction between both artificial bone and tooth in order to compare previous results carried out on live animals [1]. The implant bridges were mounted on a synthetic specimen at the first and second molar positions.

Comparably realistic and more common cases were simulated, in particularly the insertion of an implant in the site of the second molar and followed by the placement of a bridge between the implant and the first and the second premolars. The deformations caused by loads applied to the anterior and posterior abutment teeth were measured on the mandible and the implant by holographic interferometry.

The mandible and teeth were reproduced using new biomaterials that can thoroughly simulate the behavior of an actual live person.

The specimen shown in figure-1 was made of sintered hydroxy-apatite and glass-ceramics containing uniformly precipitated apatite and wollstonite crystals known as bioactive glass-ceramics. Glass-ceramics are ideal for artificial bone applications because they have great mechanical strength and are able to be attached directly to living bones.

Fig-1: Experimental specimen

The use of metallic dental implants coated with bioactive glass is becoming popular. Steady progress is also being made in the development of an artificial crown made of glass ceramics to repair teeth. The material's durability and close physical appearance to natural teeth make it ideal for artificial teeth.

Acrylic teeth with anatomical roots were mounted in the jaw using a resin cement material (3M™ ESPE™ RelyX™) then shaped and given a color similar to porcelain teeth; however, no special provision for retention is provided. Chemically, acrylic teeth are cross-linked modified plastic materials, pigmented for esthetics. The cross-linking reduces crazing. The gingival portion may not be as highly cross-linked in order to obtain a better bond with the denture base material. Physical properties of acrylic teeth, compared to porcelain teeth show high resilience rather than brittleness. They are tough, have low resistance to abrasion, are nearly insoluble in oral fluids, have dimensional change, low heat distortion temperature and flow under pressure. Acrylic teeth are used as tooth replacements in the same manner as porcelain teeth. The main working differences are wearing away more rapidly when grinding for adjustment and the lower thermal productivity. Generally, acrylic denture teeth are used in cases where intra-occlusal space is limited, in cases where they oppose other acrylic teeth or in cases of patient preference.

Optical Technique

Using the holographic interferometry technique, the presence of speckles is required since they encode displacement information. To obtain ideal conditions the speckle visibility must be optimized. The speckle visibility depends on many variables and requires a complex statistical analysis. However, a simple model can be used to ascertain the main variables influencing the visibility of speckles. The intensity at a point of the image of a rough object illuminated with laser light is given by:

$$I(r') = \left[\int_A k(r,r') A(r) e^{i\phi(r)} dA \right]^2 \qquad (1)$$

Where r is the polar coordinate of the point of the object, r' is the polar coordinate of the same point in the image plane, the term A(r) $e^{i\phi(r)}$ represents the object field and k (r,r') represents the spread function of the imaging system. The spread function defines the region of the object that influences the image of a point r'. It depends on the geometry of the lens aperture and on the lens properties including lens aberrations. The changes in amplitude and phase of the object wave front in the region of influence determine the visibility of the speckle field. Looking back at (1) it is possible to see that the visibility can change by modifying the surface properties. The spread function k (r,r') can be modified by changing the aperture geometry and the lens properties. If the recording is made using a CCD camera, settings can be changed to optimize speckle contrast. The outcome of electro-optical interferometry is influenced by a number of basic properties. The displacement resolution or minimum displacement that can be measured depends on the configuration of the optical system and the wavelength of the illumination light.

For example, if we are interested in the in-plane displacement using double beam illumination, the sensitivity is:

$$\Delta d = \frac{\lambda}{2 \sin \alpha} \qquad (2)$$

Where □ is the wavelength of the illumination light, □□is the angle of the illumination beams with respect to the normal surface that is at the same time the direction of observation. As a rule, the higher the magnification is, the larger the sensitivity required. If we apply the Rayleigth criterion, the radius of the Airy disk gives the resolution:

$$\Delta r = 1.22 \frac{\lambda}{2NA} \qquad (3)$$

Where □ is the wavelength of the illumination light, NA= sin □ is the numerical aperture of the lens, and □□□□□is the half cone entrance angle of the lens. As an alternative to observing the diffraction pattern of a point we can express the image resolution in terms of a periodic grating. In such case the resolution will be given by:

$$\Delta r' = \frac{\lambda}{2NA} \qquad (4)$$

The optical interferometer shown in figure-2 is composed of a He-Ne laser whose beam goes to a 50 percent beam splitter that produces two collimated beams. These two sources provide illumination in one direction. The signal detection is performed by a CCD camera. The observed region has a projected width of approximately 5cm.

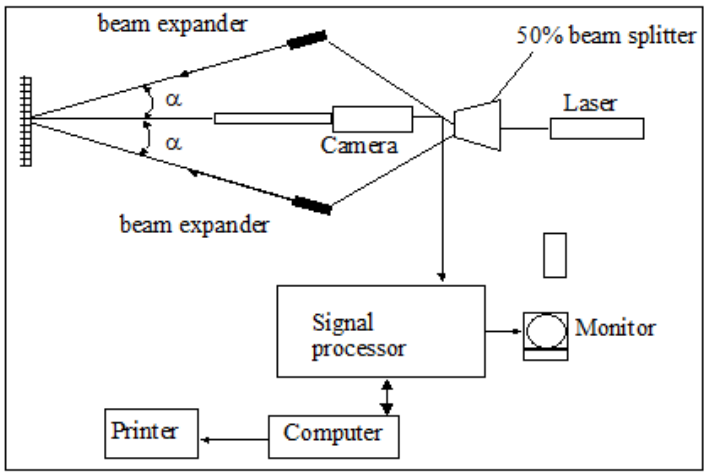

Fig-2: Optical set-up

The signal processing system contains electronic components that are needed for fringe generation and fringe analysis. There is a monitor to observe the collected images, the fringes and the intermediate steps of fringe processing. The host processor is a PC that inputs the necessary commands to the system and handles some of the final tasks required to provide the output signals. The Holo-Moiré strain analyzer uses ESPI that can be classified as focused image holography [2]. Electronic-holography obeys the classical equation:

$$n\lambda = \mathbf{d} \bullet \mathbf{S} \qquad (5)$$

Where n is the fringe order, λ the wavelength of light, **d** the displacement vector and **S** the sensitivity vector. Since there are two illumination beams, one acts as reference beam for the other therefore not requiring a separate reference beam. The sensitivity of the system is given by:

$$u = \frac{\lambda}{2\sin\alpha} \qquad (6)$$

Where u is the displacement in the direction of the x-axis, α is the angle that the illumination directions make with the direction of observation. In this case $\alpha=20^{o}$ and the sensitivity u = 0.925 μm.

The speckle correlation technique consists of adding an image shift between the two exposures (unloaded and loaded) [3-6]. As described in [4] after filtering in the frequency space a system of carrier fringes is observed in the region under analysis. To obtain the actual displacement field it is necessary to remove the carrier fringes. The desired result was achieved in the following way: first, the wrapped phase of the carrier fringes was computed. Then the carrier fringes were recovered by reducing the size of the filter in the frequency space in such a way that only one frequency was obtained. We then subtracted the wrapped phases of the two systems of fringes. By doing this, the wrapped phase of the displacement information was obtained. Finally, the strains were computed from the wrapped phase of the fringes by using the technique described in [4].

Deformations before Bridge Installation

Figure-3 shows the reconstruction images of the teeth and mandibular bone subjected to the vertical load of 8N.

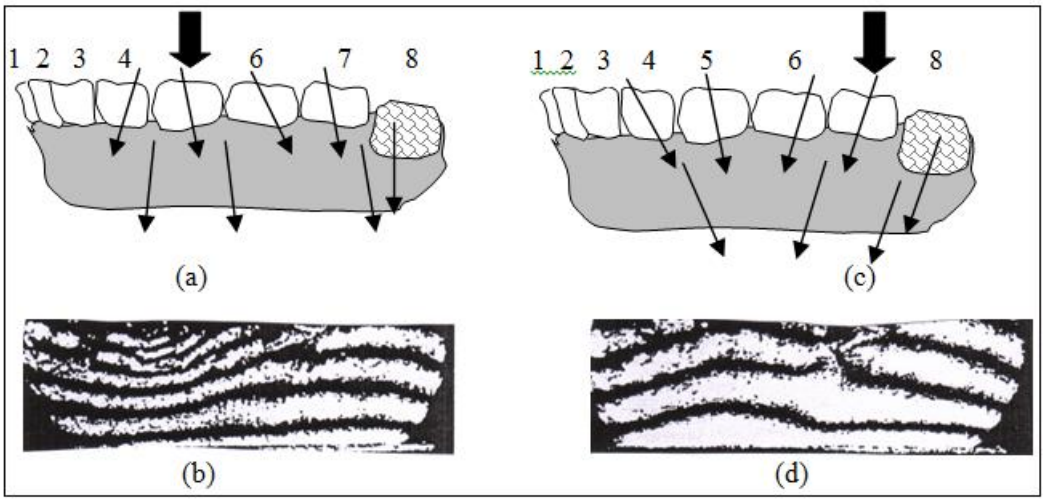

Fig-3: Schematic load application on natural teeth and interferometric fringes

Figures 3a and 3c show the deformation obtained by the vertical load concentrated on the second premolar 5 and second molar 7 respectively. In figures b and d the direction of deformations are shown related to the previous cases. A factor worthy of note is that when analyzing image 3a, it is evident that the mesiobuccal surface of the second premolar shifted considerably more than the distalbuccal ones and its mesial proximal surface becomes extremely close to the distal proximal surface of the first premolar (4).

Deformations after Bridge Installation

The first and second premolars were splinted together and then connected to the second molar using a classic bridge. Figure 4 shows the results of the experiment. In figure-4 a the vertical load was applied to the second premolar 5 and the holographic fringes were inclined to the right.

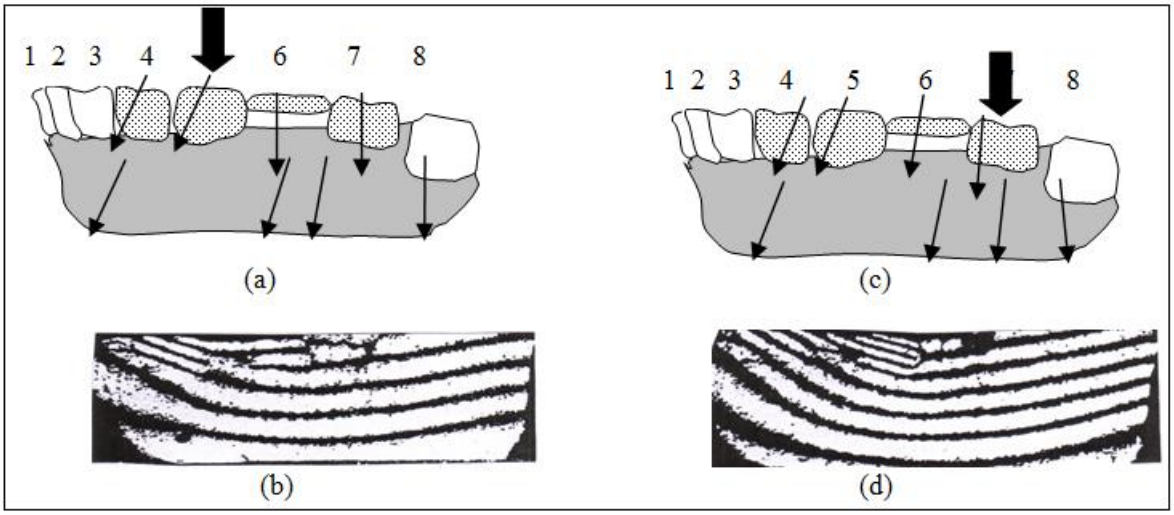

Fig-4: Schematic load application on natural teeth and interferometric fringes (bridge)

Due to the fact that the distal side of the tooth 5 does not have any constraint point, it was free to move considerably more than the mesial side which on the contrary was connected and obstructed by the pontic as shown in figure 4a. When the vertical load was considered on tooth 7 as shown in figure 4c, its distal side moved more than the mesial side and the fringes on the entire bridge slanted easily. All were regular from the premolar 4 to the molar 7 for both cases of loading position. This means that the bridge deformed as an entire body and its density was bigger than the mandible's density.

Deformations after Bridge and Implant Installation

Figure-5 shows the deformations obtained by loading teeth 5 and 7 respectively. By analyzing the fringes in figure 5a, it can be easily seen that the fringes slope on the teeth turns in the opposite direction between the tooth and the pontic. In figure 5 c the load was applied to tooth 7 causing the distal side of the second premolar 5 to shift forward with a clear displacement of the pontic and the upper part of the implant in the same distal direction. Considering the case of the load on the tooth (5), deformations of the pontic and implant 7 were in the opposite direction of the teeth 4 and 5. On the other hand, by loading tooth 7,

the almost unidirectional deformations could cause consistent damage to the mesial side of the pontic especially in the case of continuous and long work in those conditions.

The bone resorption near the implant could also cause further damage eventually caused by a large strain due to the masticatory forces applied to the bridge.

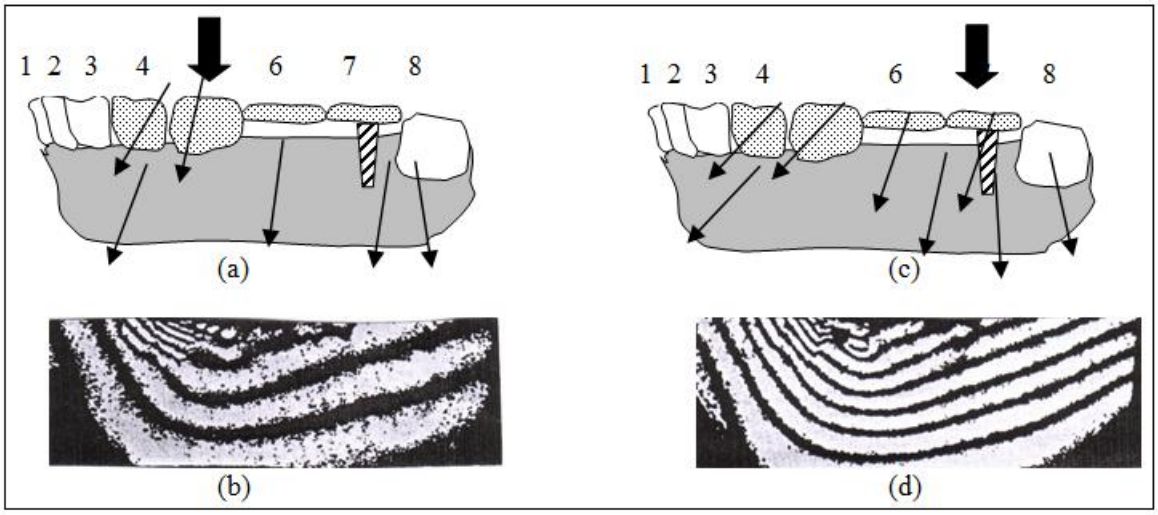

Fig-5: schematic load application on natural tooth and implant and interferometric fringes

CONCLUSIONS

In the present research, the bridge and close mandible deformation due to occlusional forces was measured by an innovative automatic holographic interferometry technique. A specimen composed of sintered hydroxy-apatite and acrylic teeth was used in order to simulate actual behavior.

Taking into consideration the implant bridge, a stress concentration was found on the mesial side of the pontic when the vertical load was applied to the second premolar. This clearly shows that the bone near the implant receives most of the stress and could suffer damage such as bone resorption, particularly when the loads are concentrated to its mesial side.

In view of the implant inserted in the alveolar bone and the experimental results obtained, it is possible to declare that its axis direction can be selected in terms of orientation as long as we do not have stress concentration on the pontic.

Different situations occur when the study is concentrated on a bridge formed on the natural teeth as the abutment teeth. What happens is that, unfortunately, it is not possible to modify the directions because they are already fixed with consequently a possible bone resorption of the mandible around the natural teeth caused by the large strain present near the implant as shown by the optical results.

REFERENCES

1. Block, M. S., Kent, J. N., & Kay, J. F. (1987). Evaluation of hydroxylapatite-coated titanium dental implants in dogs. *Journal of Oral and Maxillofacial Surgery*, *45*(7), 601-607.
2. Pappalettere, C., & Trentadue, B. (2001). Accuracy and sensitivity achieved in 3-D dental measurement using the fringe projection method. *Proc. Int. Cong. in 'Experimental mechanics (SEM)', Portland, OR, USA*.
3. Sciammarella, C. A., & Bhat, G. (1992). Two dimensional Fourier transform methods for fringe pattern analysis. In *7th International Congress on Experimental Mechanics* (Vol. 2, pp. 1530-1538).
4. Sciammarella, C. A. (1972). Use of gratings in strain analysis. *Journal of Physics E: Scientific Instruments*, *5*(9), 833-845.
5. Sciammarella, C. A., & Bhat, G. K. (1992). Computer-assisted techniques to evaluate fringe patterns. In *Laser interferometry IV: Computer-aided interferometry* (Vol. 1553, pp. 252-263). International Society for Optics and Photonics.
6. Trentadue, B. (2017). Advanced Approach for Slopes Measurement by Non - Contact Optical Technique, *Int. Journal of Engineering Research and Application*, 7(4).